Exchange interactions in mixed Yb^{3+}-Cr^{3+} and Yb^{3+}-Ho^{3+} dimers: An inelastic-neutron-scattering investigation of $Cs_3Yb_{1.8}Cr_{0.2}Br_9$ and $Cs_3Yb_{1.8}Ho_{0.2}Br_9$

M. A. Aebersold, H. U. Güdel,* and A. Hauser
Institut für Anorganische Chemie, Universität Bern, CH-3000 Bern 9, Switzerland

A. Furrer
Laboratorium für Neutronenstreuung, Eidgenössische Technische Hochschule Zürich, CH-5232 Villigen PSI, Switzerland

H. Blank
Institut Laue-Langevin, 38042 Grenoble Cedex, France

R. Kahn
Laboratoire Léon Brillouin, Centre d'Etudes Nucléaires de Saclay, 91191 Gif-sur-Yvette, Cedex, France
(Received 17 May 1993)

The two title compounds were synthesized and investigated with the inelastic-neutron-scattering (INS) technique. They contain mixed $YbMBr_9^{3-}$ ($M=Cr^{3+}$, Ho^{3+}) dimers as discrete units, and the magnetic excitations of mixed Yb^{3+}-Cr^{3+} and Yb^{3+}-Ho^{3+} dimers could thus be observed. The Yb^{3+}-Cr^{3+} dimer has three INS transitions, for which anisotropic exchange, as well as zero-field splitting of Cr^{3+}, has to be included in the exchange Hamiltonian. For the Yb^{3+}-Ho^{3+} dimer the effect of the exchange interaction manifests itself as a broadening and a splitting of the crystal-electric-field levels of the isolated Ho^{3+} ion. Taking into account the full $(2J+1)$ ground-state multiplet of Ho^{3+}, as well as anisotropic exchange, gives a satisfactory description of this dimer.

I. INTRODUCTION

The study of exchange interactions in magnetic insulators has for many years attracted a lot of attention both by physicists and chemists.[1,2] A wide range of different crystal structures is available and within a series of mixed crystals of a given structure the ratio of diamagnetic to paramagnetic ions can usually be varied. One can thus investigate the pure magnetic lattice, the properties of isolated paramagnetic ions in a diamagnetic host lattice, or isolated homo- and heteronuclear clusters of two, three, or more magnetic neighbors. The low-lying electronic energy levels of such magnetic systems are usually described by a total Hamiltonian containing the sum of the single-ion Hamiltonians for the individual ions and an exchange Hamiltonian to account for the interaction between the ions. The form most often chosen for the exchange Hamiltonian is the well-known isotropic Heisenberg-Dirac-Van Vleck (HDVV) Hamiltonian,[3] particularly for systems with well-separated spin-only ground states. Another model of great importance in the theory of magnetism, the Ising model, has been used in the case of very anisotropic systems, particularly in one- and higher-dimensional systems.[3] As experimental techniques improved, it was realized that the exchange is of a more complicated nature than described by either the HDVV or the Ising Hamiltonian.

In order to understand the basics of exchange interactions between ions in insulators, the ion pair as the most simple magnetic cluster has become the subject of many investigations. The various important contributions to the interaction in such a dimer system have been reviewed by Bencini and Gatteschi.[4] Dimers of transition-metal (M) and rare-earth (R) ions in different crystal lattices have been studied by EPR, optical spectroscopy, magnetic measurements, and inelastic neutron scattering (INS).[1-15]

In particular, spectroscopic transitions between the exchange-split components of the ground and first crystalline-electric-field (CEF) levels can often be directly observed by INS. This technique thus provides direct access to these splittings and allows a very detailed analysis in terms of theoretical models.

Compounds of the general composition $Cs_3R_2Br_9$ crystallize in the space group $R\bar{3}c$.[16] This crystal structure contains $R_2Br_9^{3-}$ dimers consisting of two face-sharing RBr_6^{3-} octahedra as discrete units with approximate D_{3h} point symmetry (the actual symmetry is C_3). The threefold dimer axis coincides with the crystal c axis. $Cs_3Cr_2Br_9$ crystallizes in the closely related space group $P6_3/mmc$.[17] The neat compounds $Cs_3Yb_2Br_9$ and $Cs_3Ho_2Br_9$ as well as the isostructural diamagnetic $Cs_3Y_2Br_9$ doped with Ho^{3+} have previously been studied by INS. Two well-resolved inelastic lines at 0.49 and 1.16 meV in $Cs_3Y_{1.8}Ho_{0.2}Br_9$ were interpreted as the $\Gamma_3\rightarrow\Gamma_2$ and $\Gamma_3\rightarrow\Gamma_3$ transitions (C_{3v} notation), respectively, within the CEF split ground-state manifold of an isolated Ho^{3+} ion in this crystal environment.[14] In $Cs_3Ho_2Br_9$ both transitions were found to be split and an exchange-tensor formalism was used to account for the energy splittings.[14] In $Cs_3Yb_2Br_9$ the HDVV model with an effective spin $S_{Yb}=\frac{1}{2}$ satisfactorily explained the observed singlet-triplet splitting,[12] and only with high-resolution

INS spectra could a small exchange anisotropy be detected.[13]

Optical spectroscopic measurements on neat $Cs_3Cr_2Br_9$ showed that bilinear exchange alone could not account for the observed behavior and biquadratic exchange was introduced.[18] INS experiments on the same compound were interpreted using a Heisenberg Hamiltonian and considering nearest-neighbor interactions between dimers in addition to the dominant intradimer exchange.[19]

Dimers consisting of two dissimilar ions, so-called mixed dimers, complicate the INS spectra substantially, but more information about the exchange can be obtained from them. Here we report results obtained on mixed Yb^{3+}-Cr^{3+} and Yb^{3+}-Ho^{3+} dimers. These are conveniently prepared by doping 10% of either Cr^{3+} or Ho^{3+} into $Cs_3Yb_2Br_9$. Their point symmetry is approximately C_{3v} (actual symmetry C_3). The two mixed dimers of this study have been chosen for several reasons. The $Yb_2Br_9^{3-}$ dimers of the host lattice have only one magnetic excitation at 0.36 meV, which is well known and well characterized.[12,13] This leaves a very large spectral range for the possible observation of magnetic excitations of the mixed dimers. Further, the single-ion properties of the three magnetic ions are well known from former work, and the effects of the exchange interactions can directly be observed by INS.

II. EXPERIMENT

$Cs_3Yb_{1.8}Cr_{0.2}Br_9$ was obtained by a slight modification of the general procedure described previously.[20] CsBr (suprapur, Merck), Yb_2O_3 (puriss 99.9%, Fluka), $CrBr_3$ (99%, Cerac), and HBr (47%, suprapur, Merck) were used as starting materials. The HBr (purum >99.8%, Fluka) gas-flow treatment to dry the intermediate product was carried out at 510 °C.

The $Cs_3Yb_{1.8}Ho_{0.2}Br_9$ sample measured at Grenoble was synthesized in the same way, using Ho_2O_3 (puriss 99.9%, Fluka) instead of the bromide as starting material. A second sample of $Cs_3Yb_{1.8}Ho_{0.2}Br_9$ was synthesized following the ammonium halide route described in Ref. 21, and was measured at Saclay.

All samples were checked by powder x-ray diffraction. They showed the correct pattern, and impurity lines accounted for less than 2% of the intensities. They were filled under He atmosphere into platelike aluminum containers of dimensions $4\times40\times45$ mm^3.

The INS experiments were performed on the time-of-flight spectrometers IN5 and IN6 at the Institut Laue-Langevin, Grenoble, and on the time-of-flight spectrometer MIBEMOL at the Laboratory Léon Brillouin at the CEN Saclay.

The instrument IN5 was used with the wavelength of the incoming neutrons set to 6.5 Å, corresponding to 1.94 meV, and giving rise to a resolution of 50 μeV at the elastic peak (EP) position. On IN6 the wavelength was set to 5.9 Å (2.35 meV) giving a resolution of 50 μeV at the EP. However, weak transitions at low energies could only be observed on IN5 and not on IN6, due to the wings from the Gaussian response function of this instrument. On the instrument MIBEMOL the wavelengths were set to 6.0 Å (2.27 meV) and 8.0 Å (1.28 meV), giving rise to resolutions of 95 and 41 μeV at the EP, respectively.

III. RESULTS

A. $Cs_3Yb_{1.8}Cr_{0.2}Br_9$

Figure 1 shows neutrons scattered from polycrystalline $Cs_3Yb_{1.8}Cr_{0.2}Br_9$ at 1.5, 5.9, and 14.4 K. The elastic peak is observed at 0.0 meV, the left-hand side of the spectrum, the energy-loss side, corresponds to the excitation of the sample by the neutron beam, and the right-hand side is the energy-gain side. The two prominent bands at ±0.36 meV can be attributed to the energy-loss and energy-gain transitions of the Yb^{3+}-Yb^{3+} dimer, respectively, which have been discussed elsewhere.[12,13] From comparison with the neat host $Cs_3Yb_2Br_9$ the two weaker bands at -1.18 and -1.05 meV, labeled I and II, can unambiguously be attributed to Yb^{3+}-Cr^{3+} dimer excitations. The observed intensity ratio of the Yb^{3+}-Yb^{3+} to Yb^{3+}-Cr^{3+} transitions is given by the ratio of the corresponding dimers in the sample. Assuming statistical distribution of the Cr^{3+} ions one expects 81% Yb^{3+}-Yb^{3+}, 18% Yb^{3+}-Cr^{3+}, and a negligible 1% Cr^{3+}-Cr^{3+} dimer.

The mixed dimer transitions show different temperature dependence. The intensity of transition I decreases with increasing temperature. The intensity of band II increases slightly between 1.5 and 5.9 K and decreases when the temperature is raised to 14.4 K, see Table I. Therefore, band I is a "cold" transition coming from the ground state, whereas band II is a transition between excited states. At 14.4 K the corresponding transitions can

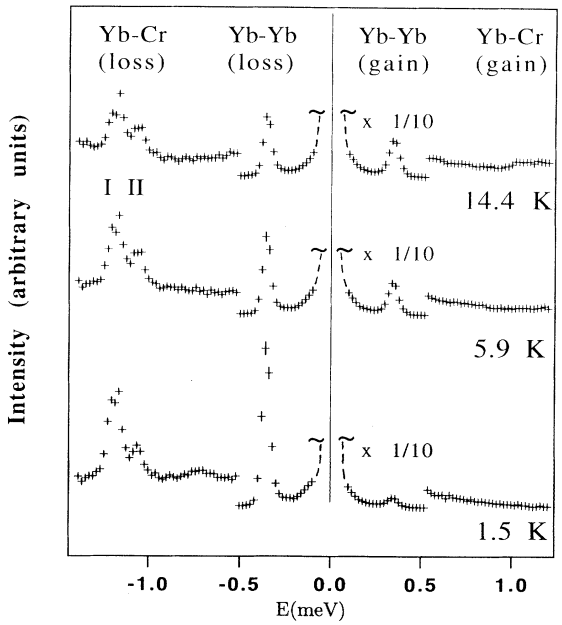

FIG. 1. Energy spectra of neutrons scattered from polycrystalline $Cs_3Yb_{1.8}Cr_{0.2}Br_9$ for the total of all scattering angles (mean $Q=1.04$ Å^{-1}). Instrument IN6, ILL Grenoble; resolution 50 μeV at the elastic peak, $\lambda=5.9$ Å.

TABLE I. Experimental and calculated temperature dependence of the two INS transitions I and II of the Yb^{3+}-Cr^{3+} dimer. For the calculation the energies and the degeneracies shown in Fig. 4(b) were used. The values at 1.5 K have been scaled to one.

		1.5 K	5.9 K	14.4 K
Transition I	expt.	1.0±0.1	0.68±0.1	0.48±0.1
(1.18 meV)	calc.	1.0	0.75	0.51
Transition II	expt.	1.0±0.1	1.39±0.1	0.88±0.1
(1.05 meV)	calc.	1.0	1.33	1.05

also be observed on the energy-gain side. The intensities of both bands as a function of the modulus of the scattering vector Q are shown in Fig. 2. Neither of the transitions shows any obvious intensity changes within the available range of $0.3 < Q < 1.6$ Å^{-1}. Figure 3 shows the low-energy part at 1.8 K measured on IN5 for $Q=0.6$ and 1.4 Å^{-1}, respectively. In addition to the Yb^{3+}-Yb^{3+} excitations another two bands labeled III are observed at ±0.12 meV, which can also be attributed to a Yb^{3+}-Cr^{3+} dimer excitation. From the intensity ratio of the energy-loss to energy-gain band it is found to be a "cold" transition. The intensity of band III decreases slightly with increasing scattering vector Q (see Fig. 2).

From the energies of the three observed transitions together with their temperature dependence, the empirical energy-level scheme shown in Fig. 4(a) is derived. The ratio of the observed energy splittings is about 1:10.

B. $Cs_3Yb_{1.8}Ho_{0.2}Br_9$

The top and middle trace of Fig. 5 show an overall view of neutrons scattered from polycrystalline $Cs_3Yb_{1.8}Ho_{0.2}Br_9$ at 1.8 K and scattering vectors of $Q=1.45$ and 0.33 Å^{-1}, respectively. The bands at ±0.36 meV correspond to the well-known Yb^{3+}-

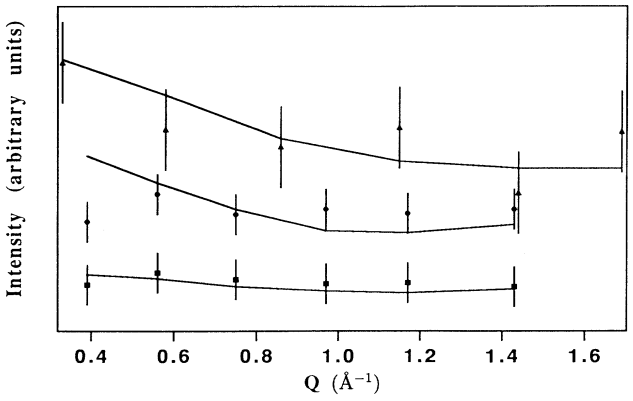

FIG. 2. Observed and calculated intensities of the Yb^{3+}-Cr^{3+} transitions I (IN6), II (IN6), and III (IN5) as a function of Q. For the calculation the procedure given in Ref. 24 was followed. The scaling of IN6 and IN5 data was done by using the common Yb^{3+}-Yb^{3+} peak. One scaling factor was refined in the least-squares fit of the calculation to the data. Calculation, solid lines. Experiment: ●, band I; ■, band II; ▲, band III.

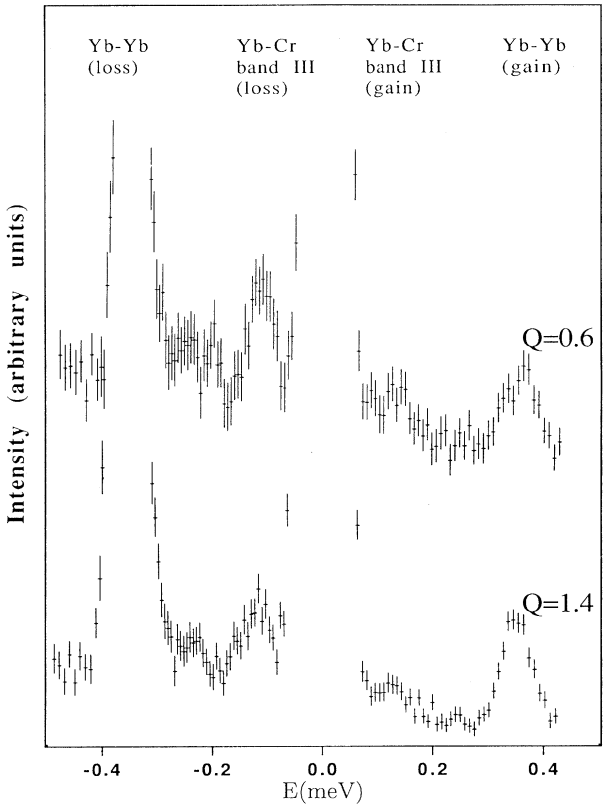

FIG. 3. Energy spectra of neutrons scattered from polycrystalline $Cs_3Yb_{1.8}Cr_{0.2}Br_9$ for $Q=0.6$ and 1.4 Å^{-1}. Instrument IN5, ILL Grenoble; resolution 50 μeV at the elastic peak, $\lambda=6.5$ Å, $T=1.8$ K.

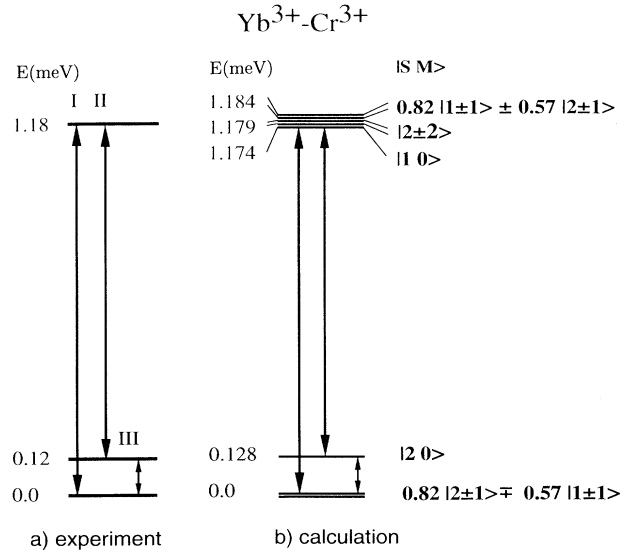

FIG. 4. (a) Empirical and (b) calculated energy-level schemes for the Yb^{3+}-Cr^{3+} dimer. The observed INS transitions are labeled and indicated by arrows.

Yb^{3+} transitions. The bottom trace shows shorter wavelength neutrons scattered from polycrystalline $Cs_3Y_{1.8}Ho_{0.2}Br_9$. From a comparison of the two upper spectra with the spectrum of $Cs_3Y_{1.8}Ho_{0.2}Br_9$ the two groups around -1.2 and -0.6 meV can unambiguously be attributed to Yb^{3+}-Ho^{3+} dimer excitations. Their center of gravity is shifted towards higher energy compared to the Ho^{3+} single-ion spectrum. The effect of the exchange coupling manifests itself in an enhanced width and a further splitting of the observed bands as compared to the well-resolved and symmetric CEF transitions in the diluted compound $Cs_3Y_{1.8}Ho_{0.2}Br_9$. The high-energy transitions at -1.23, -1.14, and -1.03 meV are labeled A, $A'+B$, and B', the two prominent bands at -0.59 and -0.48 meV are C and C', respectively. The Yb^{3+}-Yb^{3+} transition shows a very strong intensity increase with increasing Q.[12] The observed Yb^{3+}-Ho^{3+} transitions, on the other hand, show no obvious intensity changes within the available range of scattering vectors Q. Figure 6 shows the temperature dependence of these transitions. The decreasing intensity of the Yb^{3+}-Yb^{3+} band with increasing temperature is very pronounced and can be explained by a depopulation of the singlet ground state.[12] Bands A and $A'+B$ also decrease with increasing temperature. The temperature dependence of the transitions C and C' is not quite obvious from this figure. On the energy-gain side they are observed as weak shoulders on the Yb^{3+}-Yb^{3+} band both at 1.7 and 7.5 K. At 7.5 K the higher excited states are populated and the corresponding transitions A, $A'+B$, and B' appear on the energy-gain side, too. In Fig. 7, bands C and C' are

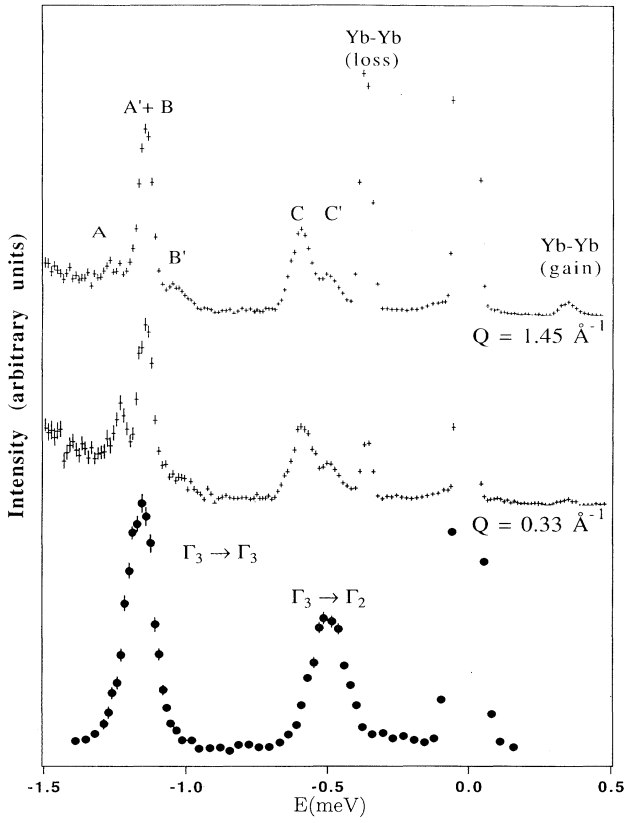

FIG. 5. Top and middle trace: Energy spectra of neutrons scattered from polycrystalline $Cs_3Yb_{1.8}Ho_{0.2}Br_9$ for $Q=0.33$ and 1.45 Å^{-1} at $T=1.8$ K. Instrument IN5, ILL Grenoble; resolution 50 μeV at the elastic peak, $\lambda=6.5$ Å. Bottom trace: Energy spectrum of neutrons scattered from polycrystalline $Cs_3Y_{1.8}Ho_{0.2}Br_9$ (from Ref. 14). Instrument IN5, ILL Grenoble; resolution 124 μeV at the elastic peak, $\lambda=4.8$ Å. The labels of the CEF transitions refer to the C_{3v} point group.

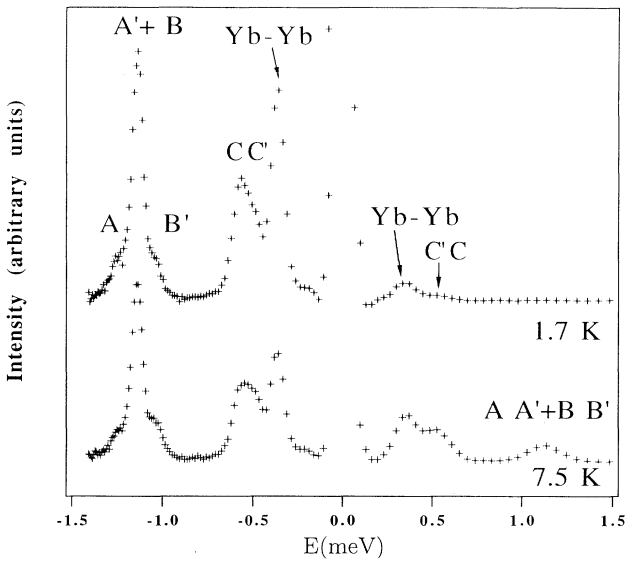

FIG. 6. Energy spectra of neutrons scattered from polycrystalline $Cs_3Yb_{1.8}Ho_{0.2}Br_9$ for the total of all scattering angles (mean $Q=1.28$ Å^{-1}). Instrument Mibemol, LLB Saclay; resolution 95 μeV at the elastic peak, $\lambda=6.0$ Å.

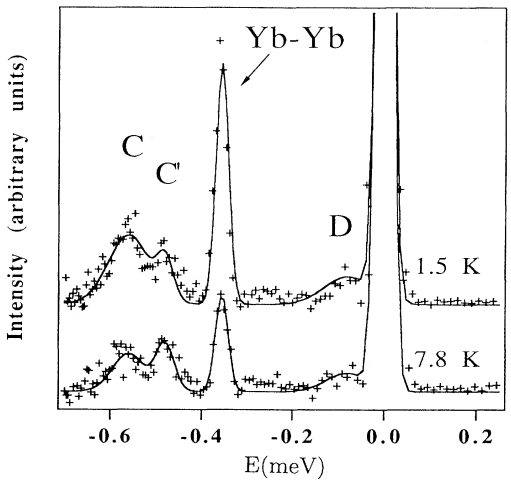

FIG. 7. Energy spectra of neutrons scattered from polycrystalline $Cs_3Yb_{1.8}Ho_{0.2}Br_9$ for the total of all scattering angles (mean $Q=0.76$ Å^{-1}) at two temperatures. Instrument Mibemol, LLB Saclay; resolution 41 μeV at the elastic peak, $\lambda=8.0$ Å. The lines are a guide for the eye.

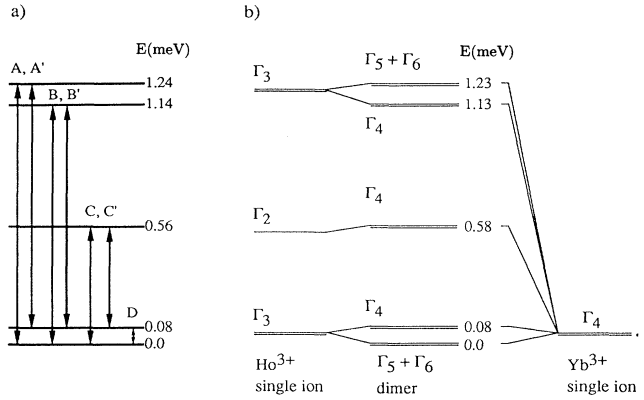

FIG. 8. (a) Empirical and (b) calculated energy-level schemes for the Yb^{3+}-Ho^{3+} dimer. The observed INS transitions are labeled and indicated by arrows. For the calculation the full Ho^{3+} ground-state multiplet was taken into account. Only the five lowest dimer states are shown.

shown at the higher instrumental resolution for 1.5 and 7.8 K. Clearly the intensity of C decreases with increasing temperature, whereas the intensity of transition C' stays more or less constant. In addition, a fourth weak band at -0.08 meV labeled D is observed. It can barely be recognized as a very weak shoulder in Fig. 5. Again an empirical energy-level scheme can be derived from the positions of the observed bands and their temperature-dependent intensities. Figure 8(a) shows this scheme with the observed transitions as arrows. A, B, and C are "cold" bands whereas B' and C' are "warm." A', the corresponding "warm" transition to A, coincides with band B (see Figs. 5 and 6).

IV. THEORY

A. Exchange interactions

The spin Hamiltonian describing the zero-field splitting (ZFS) of Cr^{3+} single ions in axial symmetry takes the form[3]

$$H_{\mathrm{ZFS}}=D[S_{z_{\mathrm{Cr}}}^2-\tfrac{1}{3}S_{\mathrm{Cr}}(S_{\mathrm{Cr}}+1)] . \tag{1}$$

The trigonal CEF interaction for an R ion within a given manifold of angular momentum J can be expressed as[11]

$$H_{C_{3v}}=B_2O_2^0-\tfrac{2}{3}B_4(O_4^0-20\sqrt{2}O_4^3)+\tfrac{16}{9}B_6\left[O_6^0+\frac{35\sqrt{2}}{4}O_6^3+\frac{77}{8}O_6^6\right] . \tag{2}$$

The operator equivalents O_k^q are tabulated[22] and the coefficients B_2, B_4, and B_6 are the crystal-field parameters. If the two ions in the dimer are allowed to interact, the Hamiltonian for the pair system can be written as

$$H_{\mathrm{dimer}}=H_1+H_2+H_{\mathrm{ex}} . \tag{3}$$

H_1 and H_2 are given by Eq. (1) or (2), depending on the nature of the metal ions 1 and 2. Including anisotropy but neglecting higher-order exchange, the exchange Hamiltonian $\mathbf{H}_{\mathrm{ex}}$ can be expressed as[23]

$$H_{\mathrm{ex}}=-2J\mathbf{S}_1\cdot\mathbf{S}_2-2J_zS_{z_1}S_{z_2} . \tag{4}$$

In order to conveniently cover the entire range of exchange parameters J and J_z the following parametrization is introduced:[23]

$$J=Ar,\quad J_z=A(1-|r|)\quad(|r|\le 1) . \tag{5}$$

A is in units of energy and determines the magnitude of the splitting and r is a measure of the anisotropy given by the relative magnitude of J and J_z. For $r=\pm 1$ this corresponds to the Heisenberg model, for $r=0$ to the Ising model, and for $r=-0.5$ to the xy model.

It is not possible to distinguish between splittings due to exchange interactions and magnetic dipole-dipole interactions. In fact, the latter are automatically included in Eq. (4). The classical interaction energies of two-point dipoles $\mathbf{u}_1$ and $\mathbf{u}_2$ can be calculated:[4]

$$W=(1/r^3)[\mathbf{u}_1\cdot\mathbf{u}_2-(3/r^2)(\mathbf{u}_1\cdot\mathbf{r})(\mathbf{u}_2\cdot\mathbf{r})] . \tag{6}$$

Using an interatomic distance $r=3.8$ Å,[12] we estimate for the isotropic part of the dipole-dipole interaction splittings of 1×10^{-4} meV and 0.008 meV for the Yb^{3+}-Cr^{3+} and Yb^{3+}-Ho^{3+} dimer, respectively. The corresponding splittings due to the anisotropic part are 0.017 and 0.023 meV.

B. Inelastic neutron scattering

For a detailed analysis of the dimer spectra the INS intensities as a function of the modulus of the scattering vector Q need to be calculated. The differential neutron cross section for transitions between the levels of homonuclear dimers has been given by Furrer, Güdel, and Darriet,[11] and the corresponding equations for heteronuclear dimers have been derived in Ref. 24.

V. DISCUSSION

A. $Cs_3Yb_{1.8}Cr_{0.2}Br_9$

Yb^{3+} has a $4f^{13}$ electron configuration with a $^2F_{7/2}$ ground state. Due to the trigonal crystal field, the eightfold degenerate ground state is split into four Kramers doublets. The Γ_4 (C_{3v} notation) CEF ground level is separated by 14.1 meV from the next higher CEF level.[25] Cr^{3+} has a spin-only $^4A_2$ ground state (C_{3v} notation) which is separated by almost 2 eV from the first excited state. Using effective spins $S_{\mathrm{Yb}}=\frac{1}{2}$ and $S_{\mathrm{Cr}}=\frac{3}{2}$ is therefore justified.[13] The Hamiltonian for the Yb^{3+}-Cr^{3+} dimer then takes the form

$$H_{\mathrm{dimer}}=-2J\mathbf{S}_{\mathrm{Cr}}\cdot\mathbf{S}_{\mathrm{Yb}}-2J_zS_{z_{\mathrm{Cr}}}S_{z_{\mathrm{Yb}}}+D[S_{z_{\mathrm{Cr}}}^2-\tfrac{1}{3}S_{\mathrm{Cr}}(S_{\mathrm{Cr}}+1)] . \tag{7}$$

The zero-field splitting of Cr^{3+} is usually of the order of $|0.1|$ meV or smaller. In $Cs_3Cr_2Cl_9$, a D value of -0.02

meV was reported.[26] The calculated value of 0.017 meV for the magnetic dipole-dipole interaction in the Yb^{3+}-Cr^{3+} dimer is of the same order of magnitude. The observed large splitting of 1.18 meV therefore has to be due to the exchange interaction. For the most simple Hamiltonian with $r=1$ and $D=0$, the HDVV Hamiltonian, one would expect just one transition at the energy corresponding to the triplet-quintet separation, showing the typical Q dependence for a $\Delta S=\pm 1$ transition.[27] This simple model can be ruled out for two reasons. We observe three INS transitions instead of one, and the intensities of bands I and II do not show the expected Q dependence, see Fig. 2. The Q dependence of dimer transitions is a direct probe of the amount of mixing of functions with different S quantum numbers. Bands with no obvious Q dependence must correspond to transitions between strongly mixed states. Such a mixing cannot be achieved by the ZFS term in Eq. (7) with a D value of the order of 0.1 meV. It must therefore be due to anisotropic exchange. Diagonalizing the energy matrix given by Eq. (7) as a function of the anisotropy parameter r for $D=0$ results in the energy-level diagram shown in Fig. 9(a). For $r\neq\pm 1$ the functions $|1\pm 1\rangle$ and $|2\pm 1\rangle$ are strongly mixed. This manifests itself in the nonlinear behavior of the energies of these levels as a function of r. The three other states $|2\pm 2\rangle$, $|20\rangle$, and $|10\rangle$ do not mix, and their energies as a function of r show linear behavior. Including a small single-ion anisotropy does not change the overall picture to any large extent, see Fig. 9(b). The two notable differences are the lifting of the degeneracies at $r=\pm 1$ and $r=-0.33$.

The observed energy splittings can, in principle, be reproduced with r close to 1 and around -0.33, At r close to 1 the high-energy transitions I and II would still basically correspond to $\Delta S=\pm 1$ transitions and band III to the ZFS either within the triplet or the quintet ground-state multiplet, depending on the sign of A. The intensities of transitions I and II should in this case strongly increase on going from $Q=0.3$ to 1.6 Å^{-1}, very similar to the behavior of the Yb^{3+}-Yb^{3+} peak in Fig. 5. The experimentally observed behavior is different (see Fig. 2), therefore r must be around -0.33. There are still four different energy splittings possible. Depending on the sign of A either the threefold or the fivefold degenerate sets of states is the ground state. Within these two possibilities further splittings depend on D.

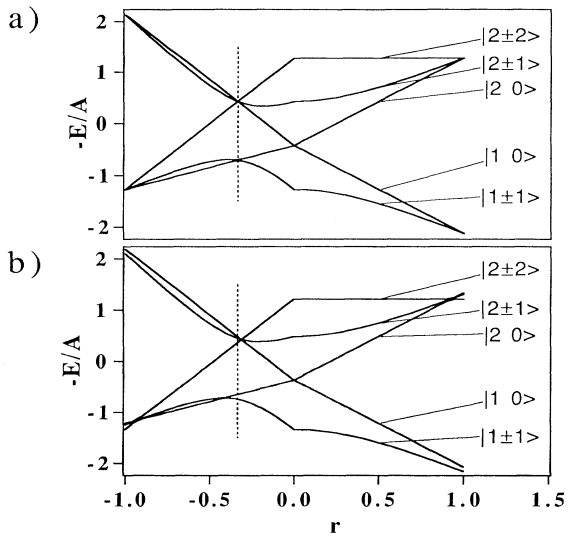

FIG. 9. Calculated energy-level diagrams for exchange-coupled Yb^{3+}-Cr^{3+} dimers according to Eq. (7) with the parametrization from Eq. (5). The dotted lines correspond to $r=-0.33$. (a) $A=-0.84$ meV, $D=0$ meV. (b) $A=-0.84$ meV, $D=-0.06$ meV.

A can be determined directly from the observed large splitting of 1.18 meV. At $r=-0.33$, A is found to be ± 0.84 meV. The observed energy splitting shown in Fig. 4(a) and the temperature dependence of bands I and II shown in Table I can be reproduced for two sets of parameters. For $A=-0.84$ meV, we find $r=-0.31$ and $D=-0.06$ meV, and for $A=0.84$ meV we find $r=-0.31$ and $D=-0.02$ meV. The first case corresponds to a twofold degenerate ground state, followed by a nondegenerate state at 0.13 meV and a fivefold degenerate state at 1.17 meV. For the second case the ground state is twofold degenerate, followed by two threefold degenerate states at 0.13 and 1.19 meV, respectively. In order to distinguish between these two models we calculated the relative intensities of the two transitions I and II, following the procedure outlined in Ref. 24. For $A=-0.84$ meV and $T=1.5$ K we obtain an intensity ratio for bands I and II of 3.7. For $A=0.84$ meV the calculation yields a ratio of 1.4. Experimentally a ratio of 3.4 is observed, in good agreement with the value obtained for the first case. With the parameters $A=-0.84$ meV, $r=-0.31$, and $D=-0.06$ meV, the following exchange and ZFS parameters are obtained:

$$J=0.26 \text{ meV},\quad J_z=-0.58 \text{ meV},\quad D=-0.06 \text{ meV}. \tag{8}$$

The energy-level scheme calculated with these parameters is shown in Fig. 4(b). A possible further splitting within the fivefold degenerate state is too small to be resolved by the INS experiment. Figure 2 shows a comparison of experimental and calculated Q dependence using the values in Eqs. (8), which is satisfactory. Experimental and calculated intensities of bands I and II as a function of temperature are shown in Table I. For the calculation the degeneracies of the three levels as shown in Fig. 4(b) were taken into account. The good agreement between experiment and calculation confirms our model.

B. $Cs_3Yb_{1.8}Ho_{0.2}Br_9$

Ho^{3+} has a $4f^{10}$ electron configuration with an $^5I_8$ ground state. In O_h symmetry the ground CEF level is Γ_3.[14] In the $Cs_2NaHoCl_6$ elpasolite the first two excited CEF levels are at 1.24 (Γ_4) and 4.8 (Γ_1) meV, and the remaining levels are well separated, lying above 24

meV.[28,29] INS spectra of $Cs_3Y_{1.8}Ho_{0.2}Br_9$ were used to determine the CEF splitting of isolated Ho^{3+} ions in C_{3v} symmetry (Fig. 5). The magnitude of the overall CEF splitting is somewhat smaller than in the elpasolite. The Γ_1 level is now at 2.95 meV and the Γ_4 (O_h) level is split into Γ_2 at 0.48 meV and Γ_3 at 1.16 meV. The remaining levels lie above 16 meV.[14] The CEF levels below 3 meV can be described as an effective zero-field split $S_{Ho}=2$ state, with the $S_{Ho}=0$ component (Γ_2) lying between the $S_{Ho}=\pm 2$ (Γ_3) and $S_{Ho}=\pm 1$ (Γ_3) components.[30]

In the mixed Yb^{3+}-Ho^{3+} dimer the Ho^{3+} CEF levels are slightly shifted to higher energies and further split, see Fig. 5. Whereas in $Cs_3Y_2Br_9$, Γ_2 is found at 0.49 meV and Γ_3 at 1.16 meV, the centers of gravity in the mixed dimer are found at 0.56 and 1.19 meV, respectively. We ascribe the larger CEF splitting to the smaller ionic radius of 87 pm in the Yb^{3+} host lattice compared to a value of 90 pm for both Ho^{3+} and Y^{3+}. Taking into account the three lowest CEF levels Γ_3, Γ_2, and Γ_3 of the Ho^{3+} ion and the Γ_4 ($S_{Yb}=\frac{1}{2}$) Kramers doublet of Yb^{3+} (C_{3v} notation) the pair Hamiltonian including anisotropic exchange is given by

$$H_{\text{dimer}}=-2J\mathbf{S}_{Ho}\cdot\mathbf{S}_{Yb}-2J_z S_{z_{Ho}} S_{z_{Yb}}+H_{Ho}\ , \qquad (9)$$

where H_{Ho} describes the ZFS of an effective $S_{Ho}=2$ state in C_{3v} symmetry. The small contributions of 0.008 and 0.023 meV to J and J_z arising from the dipole-dipole interaction calculated with Eq. (6) are automatically included in Eq. (9). Equation (9) has been diagonalized as a function of r both for $S_{Ho}=\pm 1$ and $S_{Ho}=\pm 2$ being the ground levels. Figure 10(a) shows the energy-splitting pattern obtained for $A=0.024$ meV with the $S_{Ho}=\pm 2$ level as a single-ion ground level. The Γ_2^{Ho}-Γ_4^{Yb} pair state is a single Γ_4 Kramers doublet, whereas the two Γ_3^{Ho}-Γ_4^{Yb} pair states are split into a Γ_4 and a $\Gamma_5+\Gamma_6$ Kramers doublet each [see Fig. 8(b)].

As shown in Fig. 10(a), the calculated splitting is quite insensitive to r in the range $0\le r\le 1$, and therefore the anisotropy of the exchange cannot be determined. The experimental energy-splitting pattern shown in Fig. 8 is very well reproduced with such a calculation using the parameter values $r=0.5$ and $A=0.024$ meV. However, the relative intensities of the INS transitions cannot be reproduced with this simplified model. With the $S_{Ho}=\pm 2$ single-ion ground level the calculation yields zero intensities for the transitions A, B', and C and a very weak transition C'. With the $S_{Ho}=\pm 1$ level as ground level, A and B' intensities are zero. The experiments can thus not be satisfactorily explained assuming effective spins for both ions. At least for Ho^{3+} the full $(2J+1)$ ground-state multiplet needs to be taken into account. This will lead to a further mixing of the functions, and more INS transitions between the exchange-split ground-state levels will be allowed.

For the full calculation the dimer Hamiltonian is given by Eq. (3). For Ho^{3+} the single-ion Hamiltonian from Eq. (2) was used with the CEF parameters $B_2=0.32\times 10^{-1}$ meV, $B_4=-0.5\times 10^{-3}$ meV, and $B_6=-0.12\times 10^{-5}$ meV.[31] For Yb^{3+} only the Γ_4 ground level was taken into account. Figure 10(b) shows the result of the calculation. A comparison with Fig. 10(a) shows that the overall effect of including higher CEF levels on the energy splitting is small. The range of r for which the observed energy-level splitting shown in Fig. 8(a) can be best reproduced has narrowed down to $0\le r\le 0.5$. Isotropic exchange, i.e., $r=\pm 1$, can definitely be ruled out.

The splitting pattern calculated for $r=0.25$ and $A=0.026$ meV is shown in Fig. 8(b). The experimental splittings of Fig. 8(a) are very well reproduced. The INS

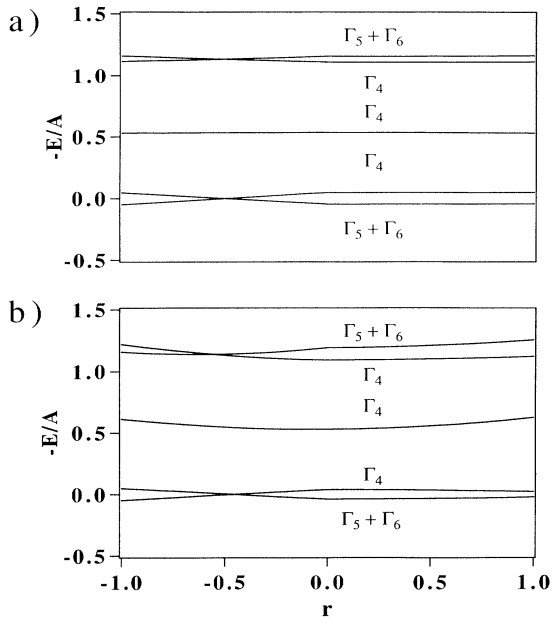

FIG. 10. Calculated energy-level diagrams for exchange-coupled Yb^{3+}-Ho^{3+} dimers according to Eqs. (3) and (9) with the parametrization from Eq. (5). The labels refer to the pair states. (a) Effective spins $S_{Ho}=2$ and $S_{Yb}=1/2$, $A=0.024$ meV. (b) Full $(2J+1)$ ground-state multiplet for Ho^{3+}, effective spin $S_{Yb}=\frac{1}{2}$, $A=0.026$ meV, $B_2=0.32\times 10^{-1}$ meV, $B_4=-0.5\times 10^{-3}$ meV, and $B_6=-0.12\times 10^{-5}$ meV.

TABLE II. Experimental and calculated INS intensities (in arbitrary units) for the Yb^{3+}-Ho^{3+} transitions for scattering vectors $Q=0.33$ and 1.45 Å^{-1}. For the calculation the procedure given in Ref. 24 was followed with $A=0.026$ meV and $R=0.25$. The experimental intensities were obtained from Fig. 5. One scaling factor was refined in the least-squares fit of the calculation to the data.

	$Q=0.33$ Å^{-1}		$Q=1.45$ Å^{-1}	
Transition	Expt.	Calc.	Expt.	Calc.
A	0.41±0.2	0.66	0.22±0.2	0.58
$A'+B$	1.35±0.2	1.64	1.58±0.2	1.08
B'	0.1±0.2	0.49	0.19±0.2	0.42
C	0.92±0.2	1.08	1.0±0.2	0.93
C'	0.41±0.2	0.59	0.43±0.2	0.44
D	0.16±0.2	0.11	0.13±0.2	0.06

intensities of the transitions have been calculated for $0 \leq r \leq 0.5$. Their variation with r is small and therefore r cannot be determined with a higher accuracy. Table II shows the experimental and calculated intensities of the various bands for $Q=0.33$ and 1.45 Å^{-1} for $r=0.25$. The agreement between experiment and calculation is satisfactory.

Whereas in the simplified model with effective spins for both ions only the energy splitting could be reproduced, the calculation with the full Ho^{3+} ground-state multiplet reproduces both the energies and the intensities of the observed INS transitions. The overall effect of including higher CEF states is small for the energy splitting but very pronounced for the wave functions. The INS intensities are very sensitive to the wave functions and therefore a direct probe for the quality of our model.

VI. CONCLUSIONS

So far only a comparatively small number of studies on mixed R-T dimers has been reported. With our Yb^{3+}-Cr^{3+} dimer we are in a comfortable situation because both the corresponding Yb^{3+}-Yb^{3+} and Cr^{3+}-Cr^{3+} dimers are very well characterized. Isotropic J values of -0.18 and -1.0 meV were reported, which correspond to total ground-state splittings of 0.36 and 6 meV in Yb^{3+}-Yb^{3+} and Cr^{3+}-Cr^{3+}, respectively. The observed total splitting of 1.2 meV in Yb^{3+}-Cr^{3+} compares very nicely with these values. There must be considerable overlap of the $4f$ wave functions of Yb^{3+} with the $3d$ wave functions of Cr^{3+}. In both Yb^{3+}-Yb^{3+} and Cr^{3+}-Cr^{3+} dimers the observed INS transitions show the typical, very pronounced Q dependence for $\Delta S=\pm 1$ transitions, and both dimers can be understood assuming effective spins $S_{Yb}=\frac{1}{2}$ and $S_{Cr}=\frac{3}{2}$, respectively. The observed Q dependence of the transitions in the mixed dimer can thus only be explained by assuming anisotropic or antisymmetric exchange. Antisymmetric exchange, the most general expression for bilinear spin-spin interaction proposed by Moriya,[32] cannot account for the observed anisotropy. By introducing a term for antisymmetric exchange in our Hamiltonian we were not able to reproduce the observed energy splittings and Q dependence. We therefore introduced the anisotropy term. The large anisotropy found, with the Cr^{3+} and Yb^{3+} spins preferably aligned antiferromagnetically along the c axis, must be due to a combination of single-ion anisotropy and anistropic exchange. We have no clear understanding why the exchange interactions in the mixed Yb^{3+}-Cr^{3+} dimer are strongly anisotropic, whereas isotropic models are adequate for the homonuclear Yb^{3+}-Yb^{3+} and Cr^{3+}-Cr^{3+} dimers.

For the Yb^{3+}-Ho^{3+} dimer an r value between 0 and 0.5 is found. Again the spins seem to align preferably parallel to the c axis. As for the Yb^{3+}-Cr^{3+} and Yb^{3+}-Dy^{3+} (Ref. 15) dimers the exchange lies close to the Ising model. This can be understood in terms of the single-ion anisotropy. For the Ho^{3+} ground CEF level Γ_3 values of $g_{\parallel}=4.1$ and $g_{\perp}=0$ are found and for the excited Γ_3 level values of $g_{\parallel}=3.6$ and $g_{\perp}=0$. The splittings of ~ 0.1 meV in the ground and excited CEF levels are of the same order as the observed splittings of ~ 0.07 meV in the ground and excited CEF levels of the homonuclear Ho^{3+}-Ho^{3+} dimer.[14]

The calculation with effective spins for both ions shows the limits of such simplified models when the ground states are not well separated. Whereas the energies of the dimer levels can more or less be reproduced, the calculated wave functions do not represent the proper dimer states. This manifests itself in the intensities of the various INS transitions. Taking the full $(2J+1)$ ground-state multiplet of Ho^{3+} a (34×34) matrix has to be solved and a satisfactory description of the dimer is obtained. If the full $(2J+1)$ ground-state multiplets of both ions are used, a (136×136) matrix has to be solved. However, the calculated energies and INS intensities are practically unaffected and therefore the assumption of an effective spin for the Yb^{3+} is well justified. As for the Yb^{3+}-Cr^{3+} dimer, we found by calculation that antisymmetric exchange cannot account for the observed energy splittings and INS intensities.

Although more work has to be done, our work shows the power of the INS spectroscopy applied to the investigation of mixed dimers. Detailed information about the exchange can be obtained. Splittings due to isotropic or anisotropic exchange can directly be observed. A complete analysis of the INS intensities as a function of temperature and the modulus of the scattering vector Q contains detailed information about the degeneracies and the wave functions of the various dimer states and thus about the anisotropy of the exchange. The well-characterized Yb^{3+}-Yb^{3+} transition always present in these mixed dimers serves as a scaling factor. It is usually observed on the energy-gain and energy-loss side and is very Q dependent. It can thus be used if the T and Q dependences of mixed dimer transitions measured on different instruments and under various experimental conditions need to be compared.

ACKNOWLEDGMENTS

We are indebted to N. Furer for synthesizing the compounds. Financial support by the Swiss National Science Foundation is gratefully acknowledged.

*Author to whom correspondence should be addressed.

[1] *Magneto-Structural Correlations in Exchange Coupled Systems,* Vol. 140 of *NATO Advanced Study Institute,* edited by R. D. Willet, D. Gatteschi, and O. Kahn (Reidel, Dordrecht, 1985).

[2] *Magnetic Molecular Materials,* Vol. 198 of *NATO Advanced Study Institute,* edited D. Gatteschi, O. Kahn, J. S. Miller, and F. Palacio (Kluwer, Dordrecht, 1991).

[3] R. L. Carlin, *Magnetochemistry* (Springer, Berlin, 1986).

[4] A. Bencini and D. Gatteschi, *EPR of Exchange Coupled Systems* (Springer, Berlin, 1990).

[5]P. J. McCarthy and H. U. Güdel, Coord. Chem. Rev. **88**, 69 (1988).
[6]J. M. Baker, R. J. Birgeneau, M. T. Hutchings, and J. D. Riley, Phys. Rev. Lett. **21**, 620 (1968).
[7]M. T. Hutchings, R. J. Birgeneau, and W. P. Wolf, Phys. Rev. **168**, 1026 (1968).
[8]H. Lueken, P. Hannibal, and K. Handrick, Chem. Phys. **143**, 151 (1990).
[9]R. B. Barthem, R. Buisson, and R. L. Cone, J. Chem. Phys. **91**, 627 (1989).
[10]N. J. Cockroft, G. D. Jones, and D. C. Nguyen, Phys. Rev. B **45**, 5187 (1992).
[11]A. Furrer, H. U. Güdel, and J. Darriet, J. Less-Common Met. **111**, 223 (1985).
[12]H. U. Güdel, A. Furrer, and H. Blank, Inorg. Chem. **29**, 4081 (1990).
[13]M. A. Aebersold, H. U. Güdel, A. Hauser, A. Furrer, M. Guillaume, and C. Carlile (unpublished).
[14]A. Furrer, H. U. Güdel, E. R. Krausz, and H. Blank, Phys. Rev. Lett. **64**, 68 (1990).
[15]M. A. Aebersold, H. U. Güdel, A. Furrer, and H. Blank, Physica B **180&181**, 206 (1992).
[16]G. Meyer and A. Schönemund, Mater. Res. Bull. **15**, 89 (1980).
[17]G. J. Wessel and D. J. W. Ijdo, Acta Crystallogr. **10**, 466 (1957).
[18]L. Dubicki, J. Ferguson, and B. V. Harrowfield, Mol. Phys. **34**, 1545 (1977).
[19]B. Leuenberger, A. Stebler, H. U. Güdel, A. Furrer, R. Feile, and J. K. Kjems, Phys. Rev. B **30**, 6300 (1984).
[20]G. Meyer, in *Inorganic Syntheses,* edited by S. L. Holt (Wiley, New York, 1983), Vol. 22, p. 1.
[21]G. Meyer, Inorg. Synth. **25**, 146 (1989).
[22]S. Hüfner, *Optical Spectra of Transparent Rare Earth Compounds* (Academic, New York, 1978).
[23]A. Furrer, H. U. Güdel, H. Blank, and A. Heidemann, Phys. Rev. Lett. **62**, 210 (1989).
[24]M. Aebersold, Ph.D. thesis, University of Bern, 1993.
[25]M. P. Hehlen and H. U. Güdel, J. Chem. Phys. **98**, 1768 (1993).
[26]J. R. Beswick and D. E. Dugdale, J. Phys. C **6**, 3326 (1973).
[27]A. Furrer and H. U. Güdel, Phys. Rev. Lett. **39**, 657 (1977).
[28]F. S. Richardson, M. F. Reid, J. J. Dallara, and R. D. Smith, J. Chem. Phys. **83**, 3813 (1985).
[29]P. A. Tanner, J. Chem. Soc. **83**, 1367 (1987).
[30]The first excited Γ_4 (O_h notation) CEF level of Ho^{3+} splits into Γ_2 and Γ_3 in C_{3v} symmetry. For the calculation with an effective $S_{Ho}=2$ the first excited state is Γ_5 (O_h notation), which splits into Γ_1 and Γ_3. In this work we use the former notation.
[31]A. Furrer, H. U. Güdel, and M. A. Aebersold (unpublished).
[32]T. Moriya, Phys. Rev. **120**, 91 (1960).